A SIMPLE METHODOLOGY FOR SURFACE LAYER CHARACTERIZATION DURING DIABATIC EXTREMES

C. BILTOFT

West Desert Test Center, Dugway Proving Ground, UT 84022, USA

Abstract. Increased global environmental awareness has fostered widespread use of remote automated weather station (RAWS) networks to monitor meteorological conditions, and reliance on atmospheric dispersion modeling for decisions concerning pollutant dispersion. Dispersion models require as input a characterization of surface layer (SL) heat and momentum fluxes and turbulence. Characterization of these quantities requires the acquisition of flux and variance information as well as the mean winds, temperature, etc. RAWS networks should be designed to provide this information. Rugged and reliable sonic anemometer/thermometers (sonics) most nearly provide the requisite measurement capability. The sonic's capacity to resolve the smallest scales of anisotropic turbulence and the fluxes of heat and momentum is investigated. Measurement deficiencies were found during extreme stable and unstable regimes. A simple methodology for defining turbulence intermittency is presented. This methodology is shown to produce useful results over a wide range of stability, to include stability extremes where reliable Monin-Obukhov Similarity (MOS) estimates are unachievable.

Keywords: Surface layer, Monin-Obukhov Similarity, Automatic Weather Station, Intermittency, isotropic turbulence, sonic anemometer

1. Introduction

Recent advances in communications, instrumentation, and data processing have made the use of remote automated weather station (RAWS) networks an economically viable alternative to manned weather stations. RAWS use is becoming so widespread that it was a major topic of discussion at the May 1998 World Meteorological Organization (WMO) session organized by the WMO Commission for Instruments and Methods of Observation (WMO, 1998). However, the Commission noted that user needs, measurement requirements, and system performance characteristics are not adequately identified. They also recommended the sharing of sensor and algorithm information and urged closer coordination among users. Meanwhile, parallel developments are occurring in atmospheric dispersion modeling in response to increased public awareness of pollution impacts on the environment. Dispersion models are increasingly used as a basis for environmental policy decision-making. These models presently require as input some characterization or parameterization of

boundary layer turbulence and stability. The fidelity of modeling results is largely dependent on the quality and representativeness of the meteorological information used as model input. Present operational models will likely be supplanted in the 21st Century by numerical models requiring initialization using detailed flux and turbulence measurements. The dispersion modeling community therefore views with great interest the development of RAWS networks and the use therein of instruments that could provide the requisite measurements.

Quantifying the state of the surface layer (SL) is particularly important because this is where most human activity and releases to the atmosphere occur. The SL lies within the first few tens of meters above the surface, between the near-surface "wall region" where the effects of viscosity and individual roughness elements are dominant and the "outer region" where local scaling is required and/or the effects of surface stress cease to be relevant. The SL is characterized by rapidly evolving high Reynolds number ($R_M = U_\infty M/\nu$, where U_∞ is the free-stream velocity, M is the momentum deficit thickness, and ν is viscosity) shear flows and buoyancy effects. These flows have R_M O 10^6 (Klewicki et al. 1995), contain substantial anisotropic turbulence components, and produce fluxes of heat and momentum over a wide range of scales that, at least at present, cannot be adequately resolved with numerical modeling. Consequently, RAWS networks will be needed in the foreseeable future to characterize the state of the SL.

Adequate SL turbulence and flux quantification requires the use of fast-response instrumentation that produce time-synchronized measurements of velocity components

and temperature. Time-synchronized measurements across an entire RAWS network, accompanied by software development, could provide information on flux, coherence, and divergence fields that is unachievable with present networks. The solid state sonic anemometer/thermometer (sonic), with no moving parts and low maintenance requirements, is the instrument most readily able to provide the requisite measurements. This paper explores the capabilities and limitations of the sonic and presents a new analysis methodology that appears to be useful over a wide range of stability, to include conditions beyond the range where reliable Monin-Obukhov Similarity (MOS) characterizations are achievable. Topics covered include: a review of SL scaling and its limitations (Section 2); the sonic anemometer/thermometer and its measurement limitations (Section 3); description and applications of covariance quadrant analysis (Section 4-6); and conclusions (Section 7).

2. Surface-Layer Scaling Theories and Their Limitations

2.1 Monin-Obukhov Similarity

When the statistics describing the state of the SL remain fairly constant over time, key scaling quantities with units of length, time, and velocity can be used to formulate dimensionless quantities that characterize the state of the SL and the dispersion rate of material released into it. A key scale representing the transition from the SL to the outer region is the height above the surface at which the forces of shear and buoyancy balance. This height is represented by the Obukhov length (L), as defined by Obukhov (1946). A stability parameter formed by the ratio of measurement

height z to L describes the strength and sign of the diabatic influence at that measurement height. Monin and Obukhov (1954) found that many SL variables scale (collapse onto a universal curve) when defined as functions of z/L, a result that has led to the widespread use of Monin-Obukhov Similarity (MOS) theory as the primary SL analysis tool. MOS scaling requires surface roughness characterization, specification of a mean temperature ($\overline{T}$), and wind speed ($\overline{U}$), and the estimation of the vertical turbulent fluxes of momentum ($\overline{w'u'}$) and temperature ($\overline{w'T'}$), where w', u', and T' represent respectively the turbulent components of vertical velocity, alongwind velocity, and temperature.

MOS and its attendant dimensional arguments constitute the most widely accepted closure hypothesis for the dynamic equations describing turbulent flows in the atmospheric surface layer. The closure objective is to describe the mean fields of temperature, velocity, etc. and their higher moments in terms of relevant scales. Monin and Obukhov (1954) postulated that the wind profile in a homogeneous and stationary surface layer can be expressed as

$$\partial \overline{U}/\partial z = [u_*/\kappa z]\Phi_m , \qquad (1)$$

where

- z = height above the surface,
- u_* = friction velocity, a measure of vertical momentum transport,
- κ = von Karman's constant (0.4 ± 0.02),
- Φ_m = the dimensionless wind gradient (1.0 in a neutral atmosphere), and
- $\overline{U}$ = the mean alongwind velocity component.

When integrated, (1) yields the well-known logarithmic wind profile equation

$$\overline{U}\kappa/u_* = \ln(z/z_0) + \psi_m , \qquad (2)$$

where z_0 is the aerodynamic roughness length, and the diabatic influence function ψ_m is the integral of Φ_m.

Both Φ_m and ψ_m are dimensionless functions of the MOS stability parameter ζ, the ratio of measurement height z to the Obukhov length L

$$\zeta \equiv z/L \equiv -\kappa z(g/\bar{q})(\overline{w'T'}/u_*^3), \qquad (3)$$

where $\bar{q}$ is the mean potential temperature and g is gravitational acceleration. Standard methods for computing ζ include direct eddy correlation solutions of (3), or iterative solutions of (2) and (3).

2.2 MOS Uncertainties

Although MOS scaling is widely accepted, its utility diminishes in the presence of strong thermal stratification, surface roughness changes, or rapidly changing heat or momentum fluxes. These inherent MOS limitations, and the difficulties (described below) with which accurate friction velocity (u_*), $\overline{w'T'}$, and L are obtained has prompted a search for more robust methods to describe the state of the SL.

Many SL quantities, when non-dimensionalized as Φ functions, scale with ζ. However, Tennekes (1982) points out that MOS provides no guidance on the form of Φ_m or the other Φ functions. The forms of these functions must be obtained by experimentation. Consequently, boundary-layer literature is replete with empirical arguments describing the Φ functions in terms of ζ. Lo and McBean (1978) found that uncertainties introduced during application of different empirical Φ functions are

on the order of 20-40% for unstable stratification (also see Table 6.3 of Panofsky and Dutton, 1984), and substantially worse for stable stratification. These uncertainties suggest a need for improved methodologies, particularly if MOS is to be applied operationally where detailed analyses are not possible.

Of the quantities used in MOS scaling, u_* and w'T' are the most problematic. The temperature and momentum fluxes can be calculated by eddy correlation of tri-axis sonic u,v,w (longitudinal, lateral, and vertical velocity components) and speed of sound (c) data, with u_* estimated from the vertical momentum flux

$$u_* \cong (-\overline{w'u'})^{0.5} \quad . \tag{4}$$

However, limitations to the eddy correlation technique are widely recognized. Busch and Panofsky (1968) found eddy correlation methods to be unreliable when u_* is less than 0.32 m/s; and Panofsky and Dutton (1984) state that estimates of u_* and L are unreliable in the weak turbulence found during stable stratification. Analogous problems also occur in extremely unstable stratification because u_* vanishes in free convection. Part of the problem is due to measurement limitations discussed in Section 3. However, another aspect of the problem is that L is small in the presence of strong diabatic effects. When L is on the order of 1 m, MOS scaling is applicable only in a narrow layer well below typical RAWS station (2-10 m) measurement heights.

Another basic problem with the eddy correlation flux computation of $\overline{w'u'}$ and, to a lesser extent, $\overline{w'T'}$ is that the turbulent (primed) components are differences

between a sample mean obtained from a time series and the individual measurements within that time series (for example, u' = $\overline{U}$-u). These turbulent components are subject to various sampling influences (discussed in Sections 3 and 5), and are often small compared to measurement uncertainties. The net fluxes are even smaller because they are the algebraic sums of the products of these small terms. Also, the ratio of u_*^3 to $\overline{w'T'}$ largely determines the magnitude and sign of L. Uncertainties in the computation or estimation of these small quantities are compounded when these quantities are used in a ratio for z/L. Thus, wild fluctuations in the sign and magnitude of z/L, as observed in the quiescent nocturnal SL, are possible when the turbulent fluxes are small.

2.3 Local Isotropy

Kolmogorov's (1941) local isotropy hypothesis for high R_M flows, developed from L. F. Richardson's idea of a turbulence cascade, complements the similarity theory of Monin and Obukhov and provide a basis for scaling SL fluxes and turbulence. One aspect of the hypothesis is that turbulent energy extracted by shear from the mean flow cascades, without loss of energy, in an inertial subrange to smaller scales at a rate equal to the dissipation rate. The distribution of energy becomes progressively more isotropic with each step in the cascade due to the tendency of pressure forces to eliminate directional preferences in energy distribution. With sufficient scale separation, small-scale turbulent eddies become stochastically independent of the larger ones.

Boundary-layer meteorologists have seized upon the idea of an isotropic inertial subrange because it permits greatly simplified (one-dimensional) SL scaling (see, for example, Wyngaard and Cote', 1972). On the other hand, Sreenivasan (1991) is considerably less sanguine about local isotropy, finding it a doubtful proposition in the inertial subrange of realistic flows. Henjes (1998) believes that isotropy of the velocity spectrum is realized to a good approximation, while isotropy of the correlation function is not. Further, measurements by Kaimal et al. (1972) and Van Atta (1991) show that isotropy is rapidly destroyed by negative buoyancy acting on stably stratified fluids. Piccirillo and Van Atta (1997) found preferential suppression of spectral energy transfer due to negative buoyancy acting on the vertical velocity component. Shear apparently fosters vertical motions at the larger scales, but negative buoyancy suppresses the cascade of energy transfer to smaller scales.

The existence of local isotropy within the inertial subrange of SL flows and the scale at which it occurs is of considerable significance. Sub-grid scale models should work on scales of motion sufficiently small to be isotropic. However, measurements are needed to resolve the larger turbulence scales in high R_M flows. The questions to be addressed are: (1) is local isotropy realizable within the inertial subrange of buoyancy-dominated SL flows; (2) does a typical sonic have sufficient bandwidth to measure motions to the scales where local isotropy is achieved?

3. Instrumentation, Measurements and Frequency Response

3.1 The Sonic Anemometer/Thermometer

The sonic anemometer/thermometer (sonic) is the instrument most readily able to produce the time-synchronized fast-response measurements needed for MOS characterization of the surface layer, although other anemometer/ thermometer combinations can perform the required measurements if sensor response characteristics are carefully matched. A sonic consists of an acoustic array containing paired ultrasonic transducers, a system clock, and microprocessor circuitry designed to measure the time intervals between the transmission and reception of the ultrasonic pulses. The fundamental unit of measure is transit time. Given transit time and a known pathlength between the transmitter and receiver, time-synchronized wind velocity components (u,v,w) and the speed of sound c can be obtained directly from each set of transmissions between paired transducers. A sonic temperature (T), essentially equivalent to the virtual temperature (Kaimal and Gaynor, 1991), can be obtained from the speed of sound measurement,

$$T = c^2/403 \quad . \qquad (5)$$

The American Society for Testing and Materials (ASTM) Standard Practices for Measuring Surface Wind and Temperature by Acoustic Means (ASTM, 1998) provides details on the calculation of wind, turbulence, and temperature statistics from time-synchronized wind component and temperature measurements.

Applied Technologies Inc. Model RSWS-201/3A tri-axis sonics were used in this study. These instruments use co-planar orthogonal u and v transducer arrays and a separate w array to produce three-dimensional wind component and temperature

measurements at a rate of 100 times per second (100 Hz), which are averaged to 10 Hz. The acoustic array transmitter-receiver spacing is 15 cm. The instrument's 12 MHz clock speed resolves velocity resolution to within 3 cm/s. These performance characteristics are fairly typical of the sonics presently available for RAWS applications.

As with all immersion instruments, the placement of a sonic into the flow that it is designed to measure causes flow distortion around the instrument and transducer shadowing within the acoustic array. Flow distortion is a disturbance of the flow that include changes in velocity, direction, and turbulence intensity due to the immersion of the acoustic array and its supporting structures within the flow. The principal deleterious effect of flow distortion in the SL is the creation of a vertical velocity measurement bias. This effect can be reduced by minimizing obstructions around the acoustic array and by careful placement of the sonic within the flow. Transducer shadowing, a velocity deficit and increase in small scale turbulence that occurs within the wakes forming downstream of the array components, requires application of a velocity correction algorithm (Kaimal et al., 1990). However, even with compensation, flow distortion and transducer shadowing effects are always present and are of particular concern for measurements made at the extreme ends of a sonic's operating range.

3.2 Special Considerations for Vertical Velocity Measurements

Vertical velocity measurements require special consideration for two reasons: (1) vertical velocity is typically the smallest measured velocity component; and (2) the

mean vertical velocity is assumed to be zero or is set to zero during computation of vertical velocity statistics and covariance terms. Because w is small compared to u and v, cross-component contamination due to misalignment, etc., often has a disproportionately greater effect on w than on u or v. Thus, an instrument designed to measure w must have substantially stricter tolerances and alignment than one designed to obtain only the u and v components. Kaimal and Haugen (1969) find misalignment or misorientation to have especially deleterious consequences for the calculation of $\overline{w'u'}$. They recommend array orientation tolerances to within $\pm 0.1°$ for instruments used to obtain the momentum flux.

Although a zero mean vertical velocity is assumed for computation of statistical quantities involving w, non-zero mean vertical velocities often appear in data sets. Discounting errors due to flow distortion, misalignment, and misorientation, non-zero vertical velocities arise as a consequence of flow over sloping terrain and the convergence/ divergence that occurs over typical (10 to 60 min) measurement periods. Some researchers advocate a software adjustment of the acoustic array tilt angle to zero prior to computation of velocity statistics. This procedure is appropriate when the flow's non-zero mean vertical velocity is due to terrain slope (i.e., the horizontal wind is forced into a vertical angle by the slope). However, this correction is inappropriate when a mean vertical velocity exists as the result of meteorological rather than terrain-induced phenomena. Rising or sinking motions that contribute to vertical fluxes are not part of the horizontal velocity component. All of the measurements cited in this report were taken over relatively flat terrain, and the deviations of w from zero within this data set are considered to be predominately of meteorological origin.

Also, most of the mean vertical velocities were 0.1 ms^{-1} or less. Consequently, no vertical velocity axis rotations were performed to generate the statistics used in this paper.

3.3 Velocity Variance Isotropy

An instrument used to acquire turbulence data should have sufficient spectral response to resolve the anisotropic component of turbulent kinetic energy and the covariance terms used to define fluxes of heat and momentum. Whether or not an instrument has sufficient response for analysis of SL variables can be determined by an examination of representative time series spectra and cospectra. Kaimal and Gaynor (1983) describe the fast Fourier transform (FFT) that was used to process the present set of 10-Hz sonic data. This processing included block averaging, tapering, scaling to meter-kilogram-second (mks) units, and normalization by multiplying each harmonic component by its frequency. Stull (1988), Panofsky and Dutton (1984), and Kaimal and Finnigan (1994) provide additional information on time series analysis applications in the boundary layer.

A revealing way to determine the point at which velocity variance isotropy occurs is to examine ratios of the power in the vertical velocity variance P(w) to the sum of the power in the horizontal variance P(u + v) components. When turbulence is isotropic, the vertical-to-horizontal velocity component power density ratio converges to a value of 0.5. Departures from 0.5 depict the magnitude of anisotropy in the distribution of turbulent kinetic energy (tke). The scale at which tke isotropy occurs is a defining

characteristic of a flow; instruments used to define velocity variance should have sufficient spectral response to resolve motions down to this scale.

Figure 1 shows power density ratios for eight cases selected to represent a wide range of stability stratification and wind speed. These cases are identified by their dominant characteristic (high wind speed, buoyancy, or meander), followed by a single-digit indication of measurement height (m). The selected spectra include: (1) one high wind speed (> 9 ms^{-1}) case (HSpd 9); (2) two cases with moderate wind speed (~ 4 ms^{-1}) and convection (Conv 9 and Conv 2); (3) two very light wind (< 1 ms^{-1}) cases, one with convection (Conv 4) and one with extreme stability (Stab 4); (4) one very stable case exhibiting a large meander component (Mndr 9); and (5) two cases with moderate winds (~ 3.5 ms^{-1}) and stable stratification (Stab 9 and Stab 2). All but two of the power density ratio plots in Figure 1 converge towards 0.5 at frequencies between 1 and 5 Hz. The exceptions are the two most stable light wind cases (Mndr 9 and Stab 4), whose power density ratios remain respectively at 0.2 and 0.1. Kaimal et al. (1971) present a similar trend in their power spectrum ratio plots.

From the results presented in Figure 1 it is apparent that local isotropy is not a general characteristic of the inertial subrange, but is usually approached at scales between 1 and 5 Hz. Buoyancy has a significant effect on the distribution of power between SL turbulence components. The vertical component exhibits proportionally greater power than the horizontal components in extreme convection (case Conv 4), but is much weaker during stable stratification (Stab 4 and Mndr 9). Thus, the computation of power density ratios provides a quantitative measure of the

suppression of w and the breakdown in energy transfer by the pressure-velocity correlation terms of the kinetic energy budget equations that occurs in the very stable nocturnal regime. Also, the lack of convergence towards 0.5 also shows that the sonic's 10-Hz data rate

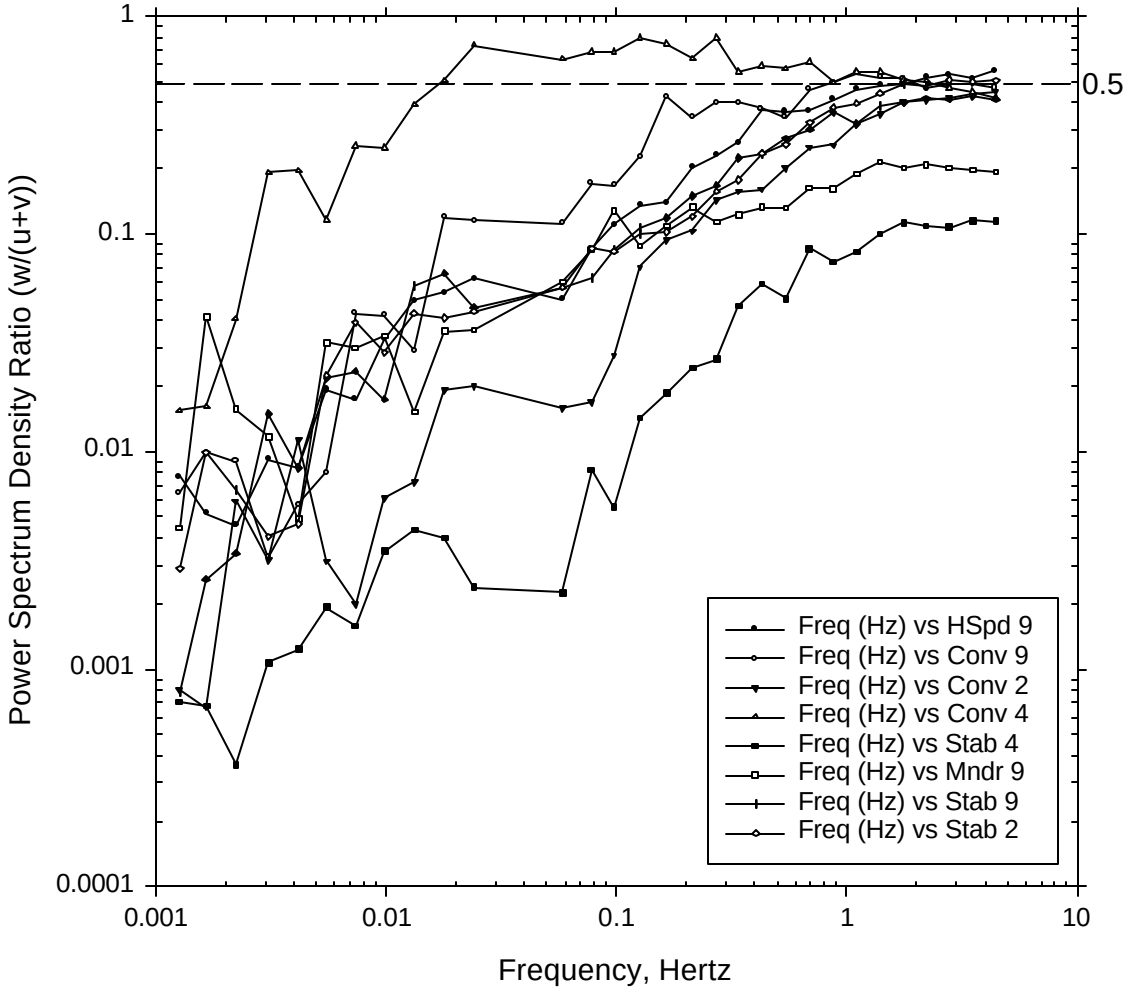

Figure 1. Power density ratio [P(w)/P(u + v)] for eight sets of spectra selected to represent a wide range of stabilities and wind speeds.

is unable to fully resolve the anisotropic portion of the velocity spectrum in the very stable boundary layer. Whether or not local isotropy is achieved in the very stable SL at scales greater than the viscous dissipation range remains an open question.

3.4 Cospectral Convergence

Another test for isotropy and instrument performance is cospectral convergence towards zero at small scales. Instrument frequency response limitations and the impact of diabatic effects on covariance terms are shown in plots of the high frequency ends of the w'u', u'c', and w'c' cospectra for the eight sample data sets, as shown in Figure 2. (Note that speed of sound was used rather than T because c is the direct result of the sonic's measurements). The w'u' cospectra (Figure 2a) also reveal the relationship between wind speed and stress on momentum flux. The magnitudes of the departures of w'u' from zero are roughly proportional to the square of the wind speed, with the greatest downward momentum flux occurring in the case with the highest wind speed (> 9 ms^{-1} for HSpd 9). Because all the cospectra converge on zero before reaching the Nyquist frequency, the transfer of momentum towards the surface in the SL appears to occur at sufficiently low frequencies that the sonic's frequency response is sufficient to adequately resolve it.

Figure 2b shows the high frequency end of the u'c' cospectra, where c' serves as a passive scalar. Diabatic effects are evident in the u'c' covariance, with the greatest negative (< 0) departures for moderately convective cases (Conv 2 and Conv 9) and the greatest positive (> 0) departures for the cases exhibiting moderately stable stratification (Stab 9 and Stab 2). The cases exhibiting the greatest unstable and stable stratification in light winds (Conv 4 and Stab 4, respectively) display near-zero cospectra, indicating weak flux contributions in very light winds. Because all of the cospectra converge towards zero for frequencies approaching the 5 Hz Nyquist

frequency, the 10-Hz sonic output again appears to be adequate for determination of the u'c' (or u'T') flux.

Figure 2c shows the high frequency components of the sample w'c' cospectra, where diabatic effects are again evident. The greatest positive flux occurs with moderate convection (Conv 2 and Conv 9), while the greatest negative flux is evident in the cases with moderately stable stratification (Stab 9 and Stab 2). Figure 2c closely resembles the inverse of Figure 2b with the following exceptions: (1) the flux for the unstable case with light wind (Conv 4) departs substantially from zero; and (2) the cospectra exhibiting the greatest diabatic effects do not converge to zero at the Nyquist frequency. The light wind unstable case indicates that, while u'c' exhibits an inverse relationship with w'c' over a limited stability range, this relationship breaks down in the presence of a strong unstable stratification. The lack of

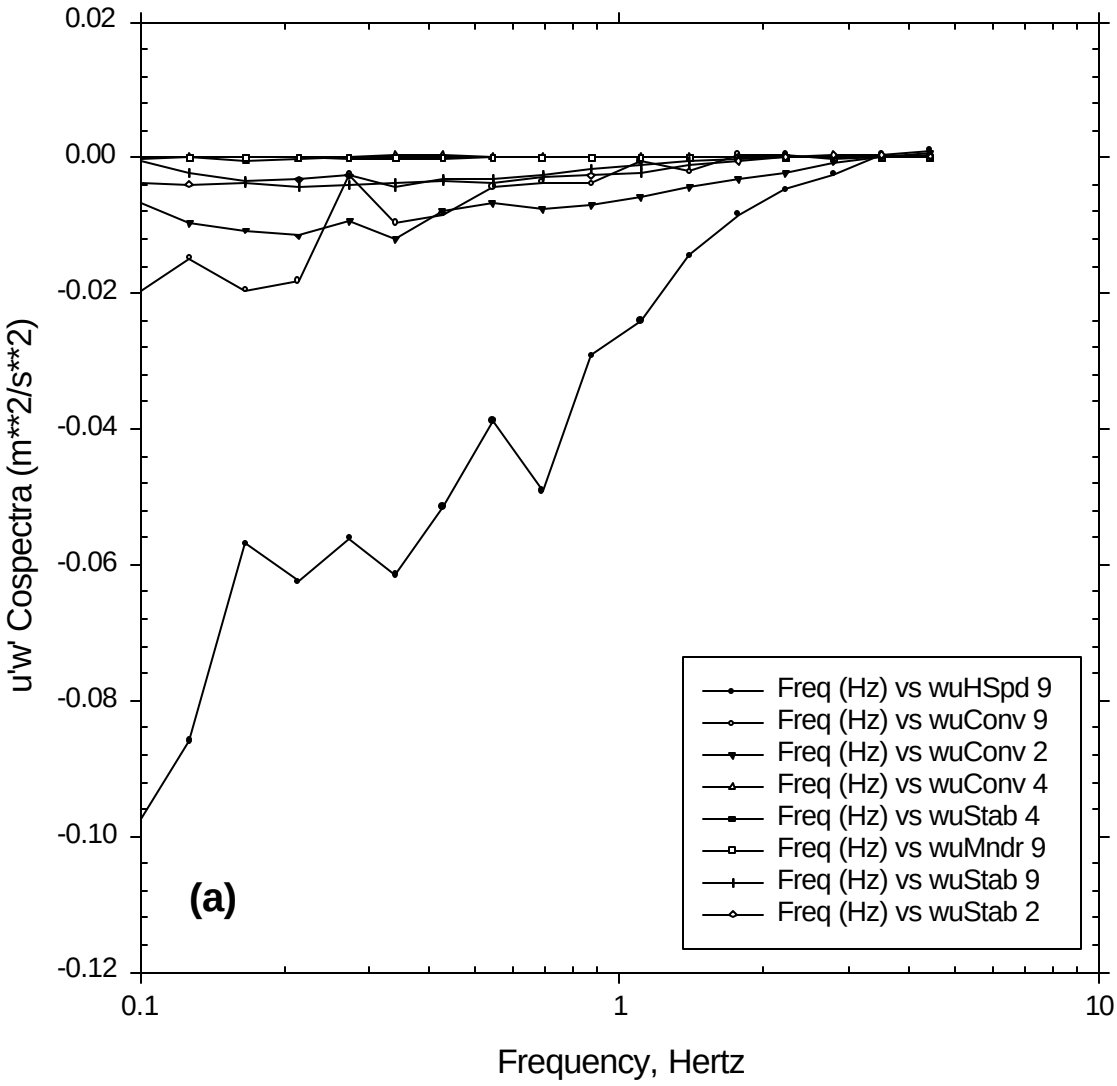

Figure 2a. High frequency (0.1 to 5 Hz) portions of the u'w' cospectra for eight selected time series.

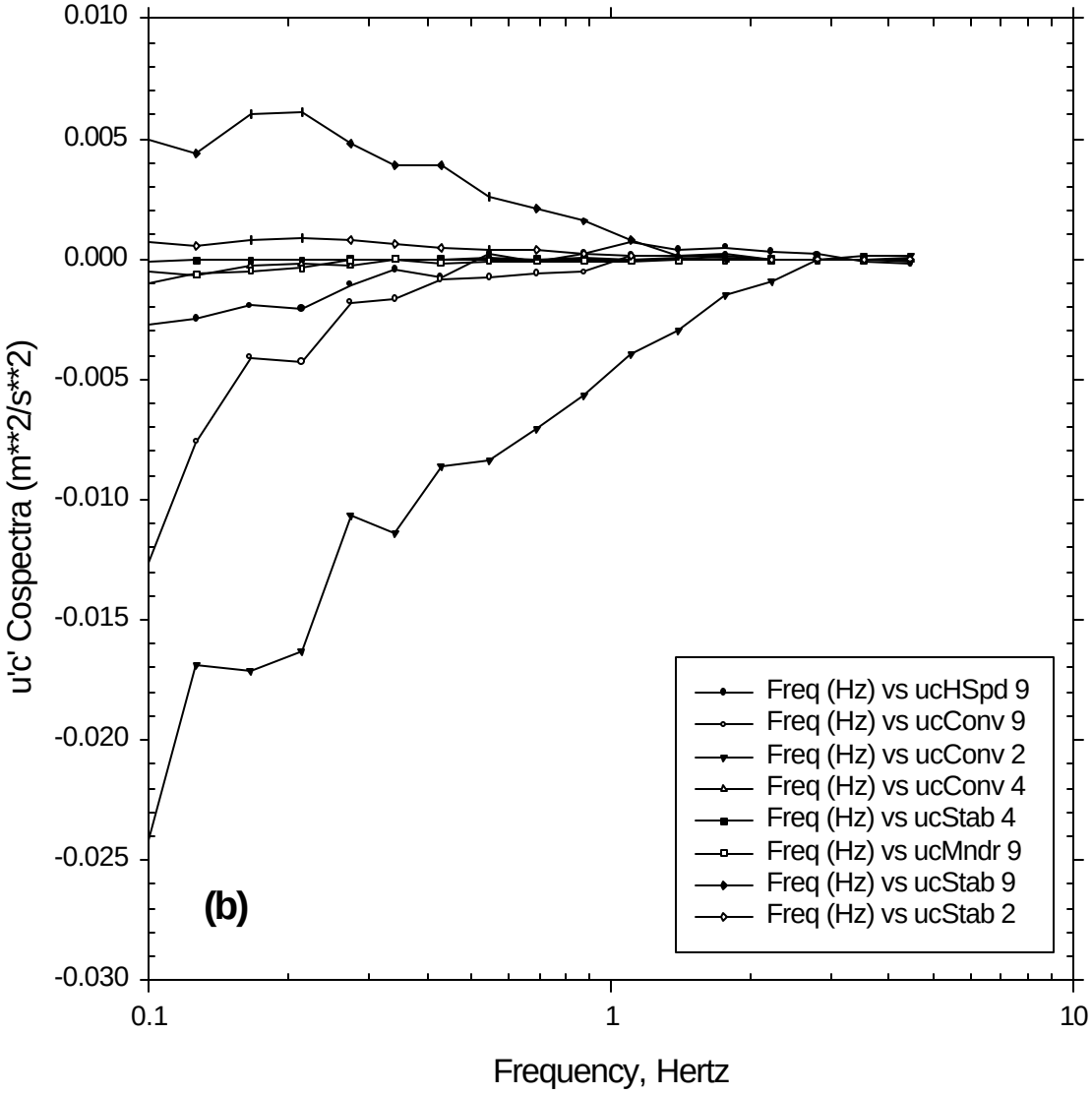

Figure 2b. High frequency portions of the u'c' cospectra for eight selected time series.

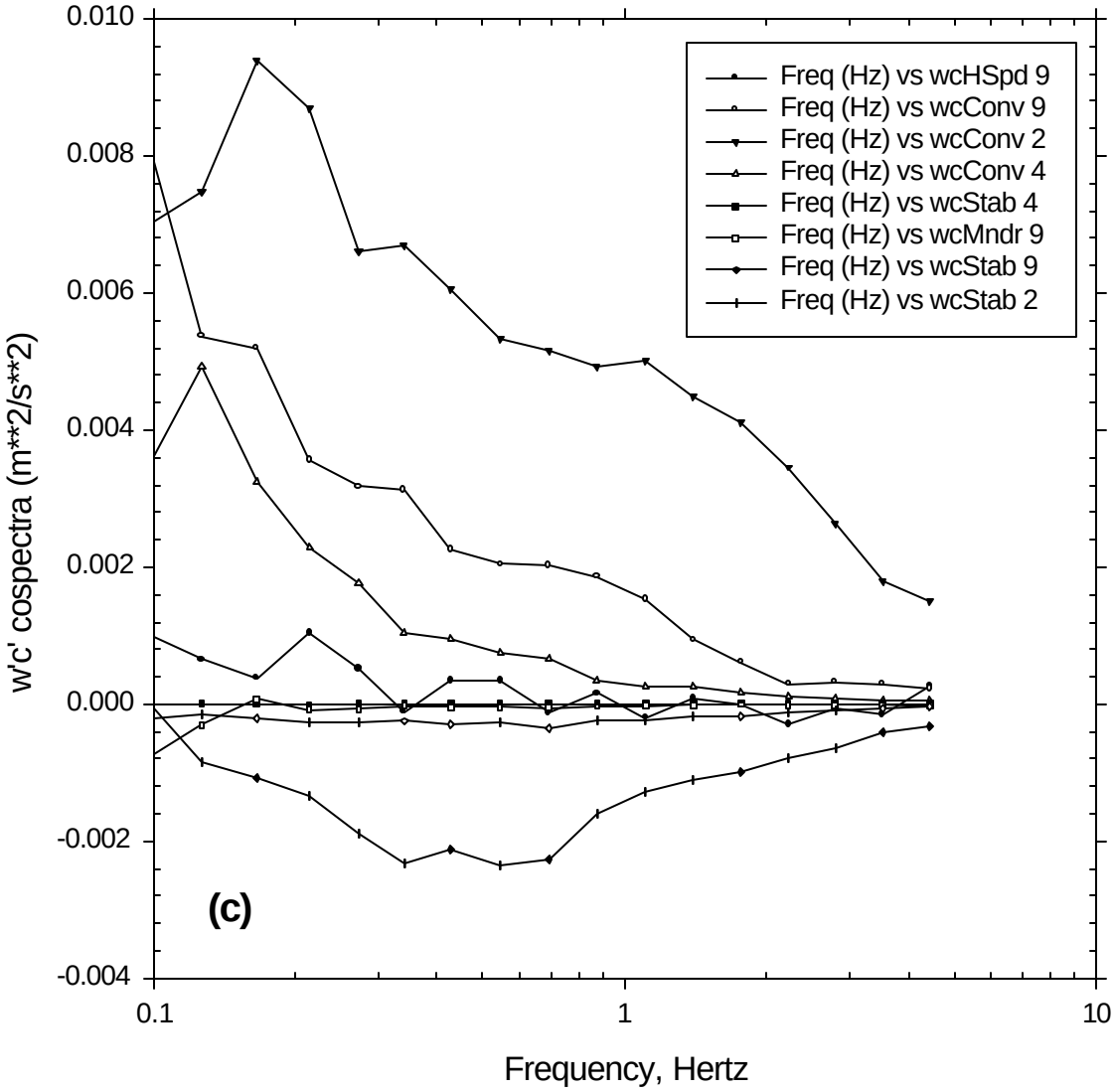

Figure 2c. High frequency portions of the w'c' cospectra for eight selected time series.

convergence on zero during convection shows that the strong correlation between temperature and vertical velocity extends to frequencies higher than 5 Hz. In consequence, a 10-Hz data rate provides insufficient frequency response to achieve isotropic convergence for the $\overline{w'c'}$ (or $\overline{w'T}$) cospectrum in extreme diabatic regimes. Improved understanding of the vertical heat diffusion and the diffusion of other passive scalars in the very stable or very unstable boundary layer will likely require instrumentation with greater spectral response.

4. Covariance Quadrant Analysis

4.1 Covariance Quadrants

In spite of the limitations to theory and measurements explored in previous sections, it is possible to obtain useful information from sonics operating in RAWS networks during extreme diabatic conditions. Covariance quadrant analysis is one under-exploited source of this information. Covariance quadrant analysis provides details of the covariance between quantity a and quantity b, where a' and b' represent the fluctuations of turbulent quantities about the means $\overline{A}$ and $\overline{B}$. Components a' and b' can be positive or negative in sign, creating four possible combinations: (1) $a' > 0$, $b' > 0$; (2) $a' > 0$, $b' < 0$; (3) $a' < 0$, $b' < 0$; and (4) $a' < 0$, $b' > 0$. If either a' or b' is near zero, the sign of the flux is indeterminate, and the contribution of a'b' to the flux is negligible. Thus, the covariance can be divided into four quadrants contributing to the flux plus a fifth indeterminate or "no-flux" region. The four quadrants and the no-flux region centered on the zero axes are shown on Figure 3. As described below, separating the covariance into its component terms can create several new analysis tools.

4.2 Net versus Gross Flux

The algebraic sum of the fractional contributions from all of the covariance quadrants yields a conventional net flux

$$Fn_{a'b'} = \overline{a'b'} \,, \tag{6}$$

while, the absolute sum of the same fractional contributions produces a gross flux

$$Fg_{a'b'} = \left| \overline{a'b'} \right| = \overline{a'b'}_g \,. \tag{7}$$

Gross flux is a measure of the total movement of a quantity "b" through the plane normal to the motion of quantity "a" without regard to the gain or loss on either side of the plane, whereas the net flux is the net migration of "b" through that plane. Thus, gross flux denotes the total distribution through the measurement plane of "b" by "a", while net flux is an indicator of source-to-sink migration. Table I displays quadrant contributions and the net and gross w'u', u'T', and w'T' fluxes for example cases with stable and unstable stratification.

The gross flux $\overline{a'b'}_g$ is a useful measure of turbulent mixing because it provides information not obtained from either the net flux $\overline{a'b'}$ or the variances (a'a' and b'b'). A useful attribute of the gross flux is that it is less sensitive than the variance terms to meander without being negligibly small due to algebraic cancellation between covariance quadrants. The gross flux is proportional to turbulent mixing because the

quadrant contributions are small only if a' or b' is small, not because the difference between the positive and negative contributions to $\overline{a'b'}$ is small. For example, consider the u'T' fluxes. The net u'T' flux could appear to be of either sign during very stable or unstable stratification because the positive and negative quadrant terms essentially cancel. At the same time, either meander or vigorous convective mixing could cause $\overline{u'u'}$ and $\overline{T'T'}$ to be large. However, $\overline{u'T'_g}$ will likely be small during stable stratification and large during unstable stratification, thereby providing greater stability discrimination than either the net flux or variance terms.

4.3 Intermittency Ratio

Given the sonic's limited capability to resolve fluxes and turbulence during diabatic extremes, a simple stability indicator that reliably discriminates between extreme diabatic regimes is needed. An intermittency ratio based on instrument performance limits serves this purpose. Because the velocity resolution threshold for the ATI sonics is ± 0.03 ms^{-1}, this value was selected as the covariance uncertainty threshold. That is, the sign and magnitude of the a'b' contribution to the covariance is indeterminate when either a' or b' are smaller than ± 0.03 ms^{-1}. This choice of 0.03 ms^{-1} as a boundary between a measurable flux and no flux is specific to the model of the instrument used. Doubtlessly, newer instruments will offer finer temporal and spatial resolution. However, choosing a different value merely shifts the scale slightly; the basic relationship between the instrument-dependent covariance uncertainty and flux intermittency remains intact.

With the establishment of an indeterminacy threshold, it is possible to define an intermittency ratio (IR). If $N_{a'b'}$ represents the total number of a'b' pairs in a data set and $n_{a'b'}$ represents the number of a'b' pairs that fall within the indeterminate region as shown on Figure 3, an intermittency ratio IR can be defined as

$$IR = n_{a'b'}/N_{a'b'} \quad (8)$$

IR can range in magnitude from 0 to 1, but in practice neither limit is achieved. Convection-enhanced turbulence produces IR values that approach zero, while strong stable stratification drives IR towards 1. Thus, IR has potential application as a simple stability indicator. The advantages of IR are: (1) it is easy to calculate; (2) intermittency ratios for the very stable and very unstable regimes differ unambiguously, even at very low wind speeds; (3) because IR is computed using thresholds rather than covariance component magnitudes, it is less susceptible to trends and meanders than are the flux terms used in conventional stability indicators; (4) it is useful even in extreme stability regimes where the sonic is not able to completely resolve the fluxes and turbulence. Thus, IR has potential application as a stability indicator in strong diabatic conditions where MOS and other stability measures fail. As an example, Table 1 lists the IR calculated for two sets of measurements taken at the same height but during different diabatic regimes. IR for the stable case $\overline{w'T'}$ ($IR_{w'T'}$) is 0.91, while the unstable case $IR_{w'T'}$ is 0.22. One could also separate covariance contributions by their intensity using multiple IR thresholds. This is a potentially useful research tool, but is beyond the scope of the present analysis.

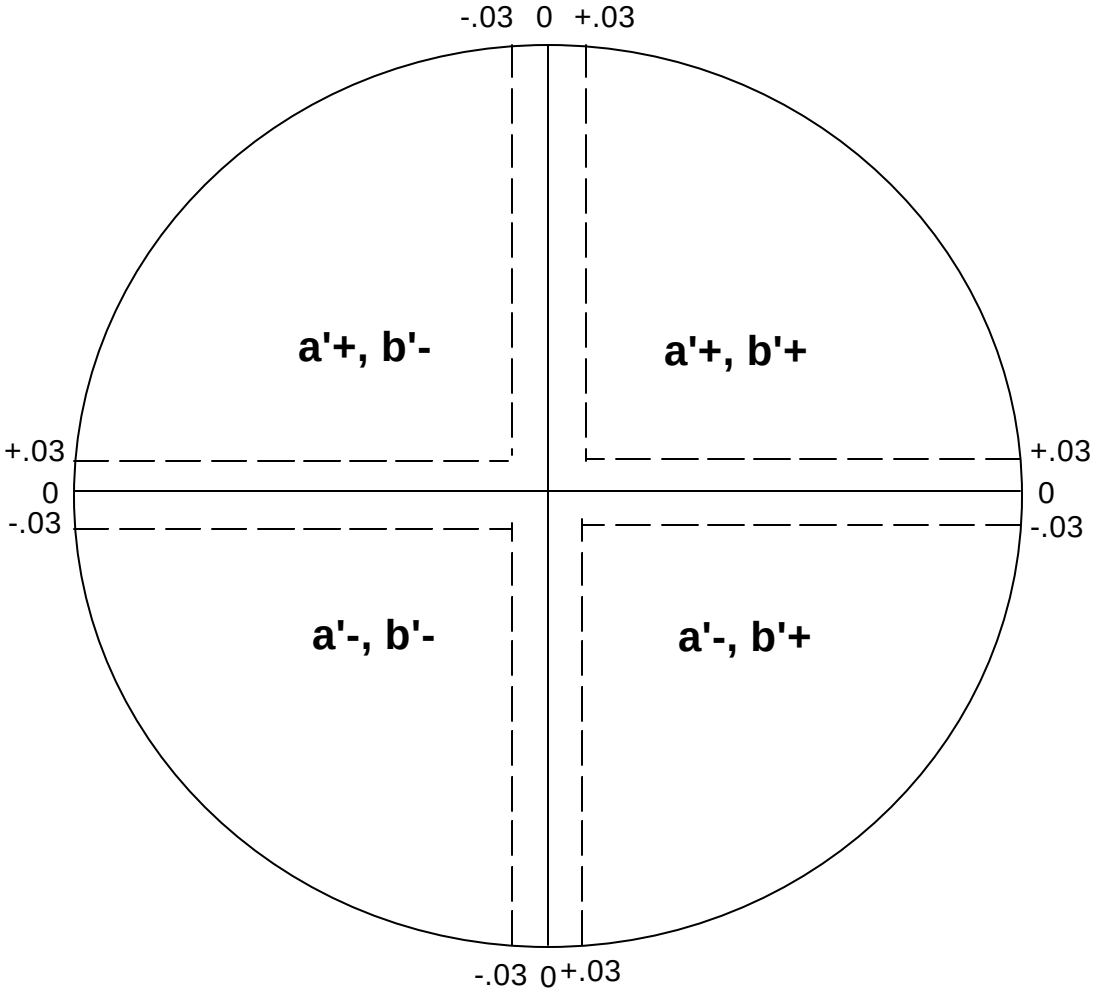

Figure 3. Covariance quadrants of ($\overline{a'b'}$) and the near-zero (±0.03) no-flux region.

Table I. Covariance Quadrant Components and Derived Quantities Obtained During Periods With Unstable and Stable Atmospheric Stratification (measurements were made in the San Joaquin Valley at a height of 4 m above ground level). In each set the upper number represents the covariance quadrant contribution, and the lower number (in parentheses) is the number of a'b' contributions to the quadrant.

Covariance Components a'b'	Covariance Quadrants				Uncertain	Intermittency Ratio	Gross Flux (mks)
	a' > 0 b' > 0	a' > 0 b' < 0	a' < 0 b' > 0	a' < 0 b' < 0	a' ~ 0 and/or b' ~ 0		
Unstable Case, L = 3.33, u_* = 0.10, $\overline{w'T'}$ = 0.0227, $\hat{U}$ = 0.8 ms^{-1}, Sample Size = 35,978							
$\overline{W'U'}$	.0138 (6181)	-.0118 (7285)	-.0129 (6643)	.0106 (7270)	.0000 (8599)	0.24	.0490
$\overline{U'T'}$	.0165 (5951)	-.0322 (9795)	-.0295 (9948)	.0272 (6560)	.0000 (3724)	0.10	.1054
$\overline{W'T'}$	.0215 (8297)	-.0061 (4721)	-.0059 (5743)	.0131 (9168)	.0001 (8049)	0.22	.0466
Stable Case, L = 250, u_* = 0.11, $\overline{w'T'}$ = -.0004, $\hat{U}$ = 1.4 ms^{-1}, Sample Size = 5,990							
$\overline{W'U'}$	.0007 (312)	-.0011 (491)	-.0002 (198)	.0001 (103)	.0000 (4886)	0.82	.0021
$\overline{U'T'}$	.0024 (1339)	-.0003 (172)	-.0000 (83)	.0022 (1180)	.0000 (33216)	0.54	.0049
$\overline{W'T'}$	.0001 (71)	-.0001 (144)	-.0003 (304)	.0000 (40)	.0000 (5431)	0.91	.0005

The disadvantage of using IR as a stability indicator is that its magnitude is height-dependent. As a consequence of its height dependence, IR reaches a maximum at the lowest part of the SL, where small-scale turbulence is nearly always present, and diminishes with height. This is consistent with observations that diffusion operates more rapidly near the surface than aloft (see, for example, Yee et al.,1995). While it functions well at diabatic extremes, the point at which IR transitions through neutral is not well defined. The magnitude of IR at the point of transition apparently increases as a function of height in proportion to $z^{1/3}$.

5. The Data Sets

The data sets used for development of the SL analysis methodology described in this paper were taken from archives of sonic data stored at the U.S. Army Dugway Proving Ground (DPG) West Desert Test Center (WDTC). A total of 100 sampling periods were chosen from five sites representing subtropical desert or steppe climates (Koppen classification BW or BS). These periods cover a wide range of wind speed (averaging 0.2 to 8.6 ms^{-1}) and stability regimes (very unstable to very stable). The measurement sites include three locations at the Department of Energy Nevada Test Site (NTS), two locations at DPG, and one location in the San Joaquin Valley. All of the sites were on flat terrain with roughness estimates varying between 0.03 cm at one of the DPG sites to 6 cm at the NTS. The NTS sites were located in basins surrounded by hilly or mountainous terrain, while the DPG sites featured flow over an open expanse of desert. The San Joaquin Valley site is typical of agricultural land in the center of California.

Because of the emphasis in this paper on operational utility, no filtering was applied to the data sets selected for the present analysis other than the occasional suppression of noise spikes. Instead, time series ranging from 6 to 60 min in duration that represented a wide range of stability regimes were selected from sonic data archives. Shorter periods were chosen for stable regimes and longer periods for unstable regimes. This 6 to 60 min. range includes sampling periods most frequently used for routine data acquisition in RAWS networks. To the extent possible, discontinuities or steep trends were avoided during data set selection. This trend avoidance procedure was most successful with the vertical velocity data and least successful with temperature data. Consequently, the statistics presented in this report contain considerably greater range and scatter than those found in data sets to which de-trending and filtering have been applied. On the other hand, the resulting data set statistics are more representative of what might be found in an operational setting where no filtering, other than that imposed by selected averaging and sampling times, is likely to be applied.

6. Gross Fluxes and Intermittency Ratio Applications

6.1 Gross Momentum flux and Vertical Velocity Variance

It was shown above that gross fluxes are easily calculated as the absolute sums of covariance quadrant components. To examine how well these indices characterize

the turbulent state of the SL, comparisons were made using $\overline{w'u'_g}$ and several other variables as predictors and vertical velocity variance ($\overline{w'w'}$) as the predictand. The evaluation began with simple linear correlations. The squared coefficient of correlation (r^2) multiplied by 100 depicts the percent of variance in the predictand accounted for by linear correlation with the predictor. Table II gives the results for several predictor-predictand pairs, and Figure 4 shows w'w' plotted as a function of w'u'. Horizontal and vertical velocity variances in Table II are represented respectively by σ_u^2 and σ_w^2, while σ_T^2 represents temperature variance.

It is apparent from inspection of Table II and Figure 4 that $w'u'_g$ is highly correlated with $\overline{w'w'}$. The $\overline{w'u'_g}$ and $\overline{w'w'}$ statistics vary over four orders of magnitude, span stability regimes ranging from very unstable to very stable, and measurement heights ranging from 1.2 to 9.5 m. Some departures from a linear relationship are evident at the very largest and smallest $\overline{w'w'}$ values. These departures are likely due to buoyancy-driven enhancement or suppression of vertical velocity discussed in Section 3. Otherwise, it appears that, on average, the $w'u'_g/w'w'$ ratio is nearly constant through the SL:

$$\overline{w'u'_g}/\overline{w'w'} \cong 1.72. \qquad (9)$$

Taking the square root of (9) and inverting yields a ratio of 0.763 that, curiously, is the inverse of the familiar $\sigma_w/u_* \cong 1.3$ found for near-neutral stability. A significant difference is that σ_w/u_{*g}, where u_{*g} is the gross friction velocity, requires no empirical

stability-dependent Φ function that is subject to the self-correlation described by Mahrt et al. (1998).

The near constancy of the $w'u'_g/w'w'$ ratio suggests that gross momentum flux might be useful for developing a simplified version of MOS. An estimate of gross friction velocity is obtained from

$$u_{*g} \cong (\overline{u'w'}_g)^{0.5} \quad , \tag{10}$$

with a gross Obukhov length defined as

$$L_g \equiv -(\theta/\kappa g)(u_{*g}^3/\overline{w'T'}). \tag{11}$$

An advantage offered by this version of MOS is that u_{*g} does not vanish in free convection, enhancing the usefulness of u_{*g} and L_g for SL scaling. Working out new MOS scaling based on u_{*g} and L_g must await a follow-on analysis effort.

Table II. Percent of the Variance in the Predictands Explained by Predictors Using the Statistical Summaries from Appendix A.

	Predictands		
	σ_u^2	σ_T^2	σ_w^2
Predictors			
U^2	22	---	46
σ_u^2	100	17	56
	---	---	---
$w'u'_g$	---	---	97
$IR_{u'w'}$	87	25	93

$IR_{u'T'}$	57	88	42
$IR_{w'T'}$	70	64	67
Eqn (12)	---	---	85
	---	---	---

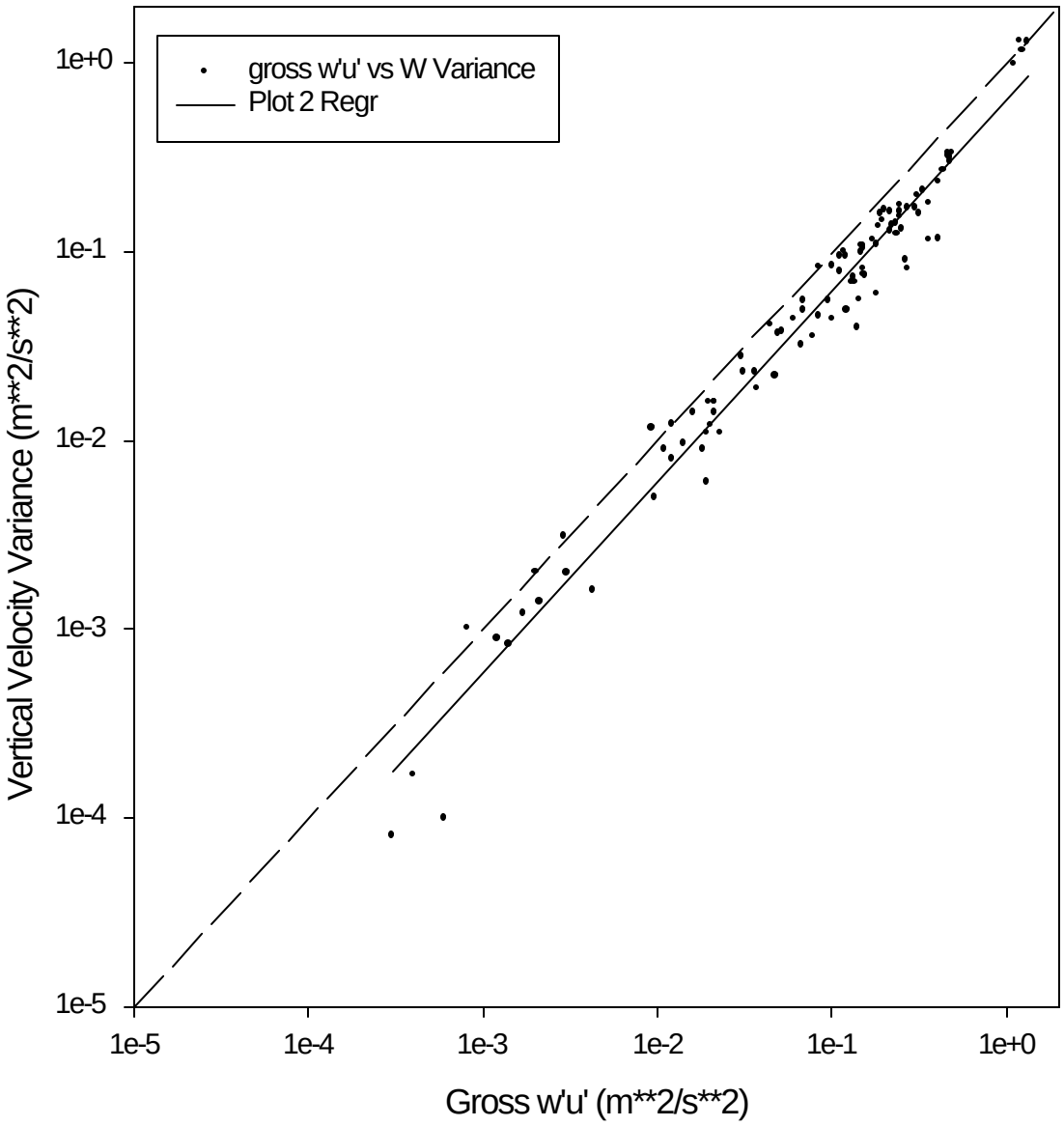

Figure 4. Plot of vertical velocity variance versus gross momentum flux ($r^2 = 0.97$). The dashed line is a 1:1 fit; the solid line is the line of regression.

6.2. Using Horizontal Components to Estimate σ_w^2

As good as the relationship between $\overline{u'w'}_g$ and σ_w^2 appears to be, it can be used only when vertical velocity measurements are available. Vertical velocity measurements are not likely to be available for many RAWS networks. However, time-synchronized temperature and horizontal wind component measurements can reasonably be expected. The strong correlation between u' and w' (shown in 6.1) suggests that useful estimates of σ_w^2 might be obtainable from time-synchronized horizontal wind component and temperature measurements. The objective now is to determine how well indices available from horizontal component data can be used to estimate σ_w^2 .

The search for simple estimation methods based on dual-axis sonic u, v, and T data began with a look at linear correlations between the predictands and candidate predictors. The correlations between the alongwind velocity, vertical velocity, and temperature variances (σ_u^2, σ_w^2, and σ_T^2) and intermittency ratios for w'u', w'T', and u'T' are shown in the correlation matrix of Table II. It is apparent that none of the possible horizontal component predictors provide a good linear correlation with σ_w^2. Therefore, various combinations of pertinent variables were used with residual analysis to minimize the unresolved variance. Residual analysis involves normalizing the predictand by a pertinent scaling variable and then reducing the variance of the residual using combinations of other variables.

The first attempt to reduce the vertical velocity variance began by dividing it by σ_u^2. The other factor contributing to reduction in error was the product of alongwind

turbulence intensity ($\sigma_u/\hat{U}$) with the $\overline{u'T'}$ intermittency ratio, $IR_{u'T'}$. The calculated vertical velocity variance

$$\sigma_{wc}^2 = 0.2(\sigma_u^2(1.-3(IR_{u'T'}\ \sigma_u/\hat{U}))) \qquad (12)$$

produced an r^2 of 0.85 when correlated with the measured σ_w^2. Vertical velocity variances calculated using (12) versus measured σ_w^2 are shown in Figure 5. Although Figure 5 exhibits substantially more scatter than the results in Figure 4, (12) does show substantial utility as a vertical velocity variance estimator.

The performance of (12) was evaluated using the geometric mean variance error (VG), a measure of relative scatter (Hanna,1993), as a figure of merit:

$$VG = \exp\left[\overline{(\ln(\text{measured}) - \ln(\text{predicted}))^2}\right]. \qquad (13)$$

The evaluation produced a VG of 1.71 (1.0 being perfect agreement) which is a reasonable expectation for a model algorithm. Also, 72% of the calculated vertical velocity variances fell within a factor of 2 of the measured values.

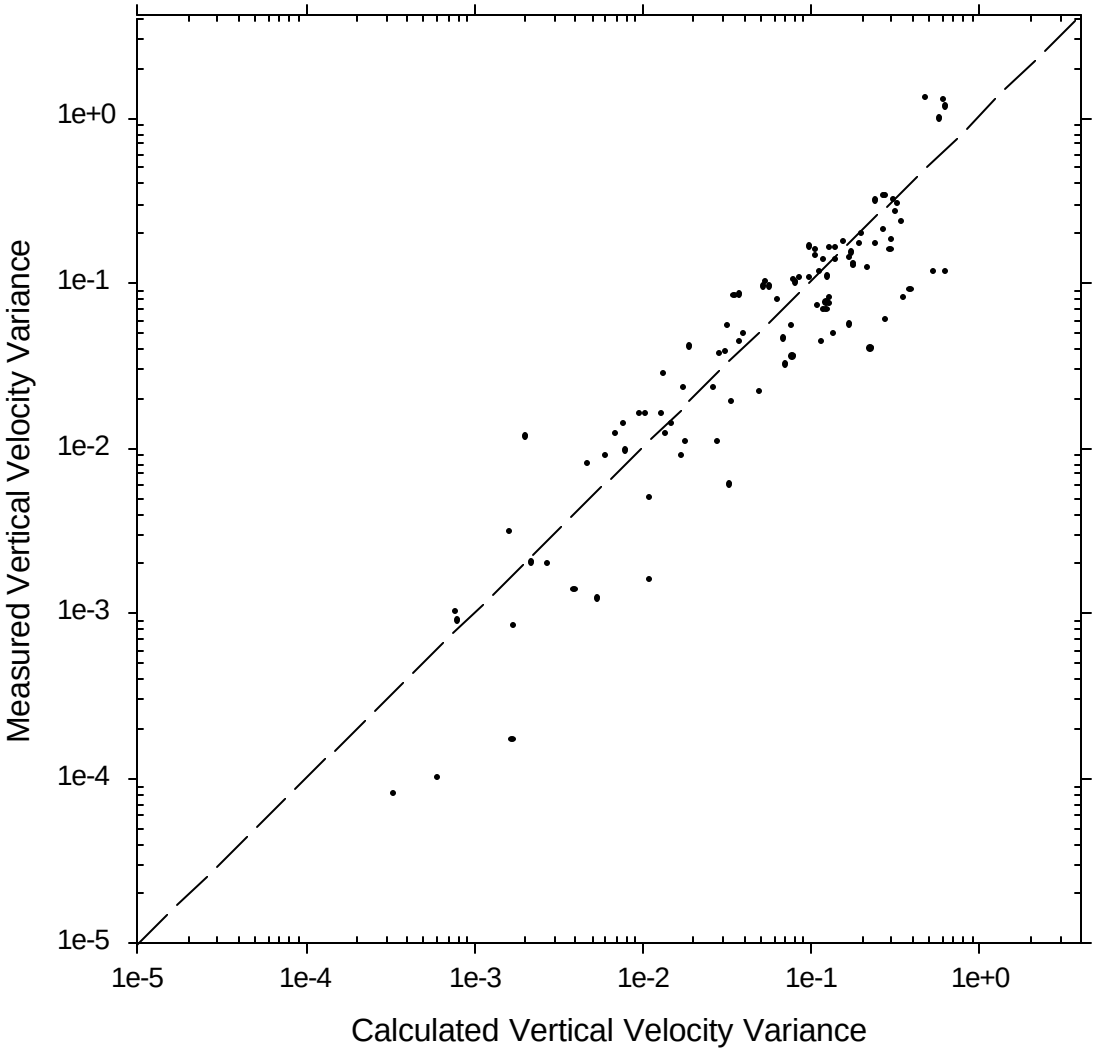

Figure 5. Measured Vertical Velocity Variance vs Estimates Calculated Using (12).

7. **Conclusions**

This paper has presented some applications and limitations of sonic anemometer/ thermometers in surface-layer RAWS networks. A RAWS network with time-synchronized measurements can function like a large distributed instrument rather than as a collection of isolated instruments, providing a great deal more information than is available from current weather station networks.

Instruments designed for flux and turbulence measurements should be able to resolve the anisotropic components of turbulence spectra. Tests reveal that convergence towards local isotropy in the surface layer typically occurs at frequencies between 1 and 5 Hz, but anisotropic effects extend to higher frequencies in the presence of strong buoyant enhancement or suppression. In consequence, measurements produced by a typical 10 Hz sonic cannot be used with Monin-Obukhov similarity to adequately describe the state of the surface layer during extreme diabatic regimes. The isotropy tests presented in this paper could also be used to evaluate the performance instruments designed for the measurement of surface-layer turbulence.

With covariance quadrant analysis, it is possible to define quantities such as gross fluxes and intermittency ratios that are useful for estimating surface layer characteristics during extreme diabatic regimes. The gross momentum flux is strongly correlated with the vertical velocity variance; the $w'u'_g/w'w'$ ratio is observed to remain constant at 1.72 over a wide range of stability conditions. Reasonable vertical velocity variance estimates can also be obtained from horizontal wind components and temperature. Even during extreme diabatic regimes where present measurement

systems are deficient, the intermittency ratio provides a simple and unambiguous measure of stability. These adumbrated methodologies provide a basis for simplified surface layer scaling, with particular application to RAWS network data used for dispersion modeling.

Acknowledgments

The author acknowledges the assistance of David Petrie (Dugway Proving Ground, West Desert Test Center), Bruce King (Western Research Institute), and David Pankratz (AeroVironment, Inc.) with data set acquisition. Dr. Walter Bach of the U.S. Army Research Office, Dr. Joseph Klewicki from the University of Utah Department of Mechanical Engineering, and Mr. James Bowers of the U.S. Army Dugway Proving Ground West Desert Test Center provided valuable critical comments on drafts of this paper. Mrs. Susan Gross provided word processing support.

References

ASTM D 5527-94: 1998, 'Standard practices for measuring surface wind and temperature by acoustic means, *1997 Annual Book of ASTM Standards, Volume 11.03, Atmospheric Analysis; Occupational Health and Safety; Protective Clothing.* American Society for Testing and Materials, 100 Barr Harbor Drive, West Conshohocken, PA 19428.

Busch, N.E. and Panofsky, H.A.: 1968,'Recent Spectra of Atmospheric Turbulence', *Quart. J. Roy. Meteorol. Soc.* **94**, 132-148.

Garratt, J. R.: 1992, *The Atmospheric Boundary Layer*, Cambridge University Press, U.K., 316 pp.

Hanna, S.R.: 1993, 'Uncertainties in Air Quality Model Predictions', *Boundary-Layer Meteorol.* **62**, 3-20.

Henjes, K.: 1998, 'Justification of the Inertial Dissipation Technique in Anisotropic Mean Flow', *Boundary-Layer Meteorol.* **88**, 161-180.

Kaimal, J.C. and Haugen, D.A.: 1969, 'Some Errors in the Measurement of Reynolds Stress', *J. Appl. Meteorol.* **8**, 460-462.

Kaimal, J.C., Wyngaard, J.C., Izumi, Y. and Cote', O.R.: 1972, 'Spectral Characteristics of Surface-Layer Turbulence', Quart. J. Roy Meteorol. Soc. **98**, 563-589.

Kaimal, J.C. and Gaynor, J.E.: 1983, 'The Boulder Observatory', *J. Climate & Appl. Meteorol.* **22**, 863-880.

Kaimal, J.C., Gaynor, J.E., Zimmermann, H.A. and Zimmerman, G.A.: 1990, 'Minimizing Flow Distortion Errors in a Sonic Anemometer', *Boundary-Layer Meteorol.* **53**, 103-115.

Kaimal, J.C. and Gaynor, J.E.: 1991, 'Another Look at Sonic Thermometry', *Boundary-Layer Meteorol.* **56**, 401-410.

Kaimal, J.C. and Finnigan, J.J.: 1994, *Atmospheric Boundary-Layer Flows*, Oxford University Press, U.K., 289 pp.

Klewicki, J.C., Metzger, M.M., Kelner, E. and Thurlow, E.: 1995, 'Viscous Sublayer Flow Visualizations At $R_\theta \cong 1500\,000$', *Phys. Fluids* **7**, 857-863.

Kolmogorov, A.N.: 1941, 'The Local Structure of Turbulence in Incompressible Viscous Fluid for Very Large Reynolds Numbers', *Dokl. Akad. Nauk SSSR* **30**, 299-303. (English transl. In 1991, *Proc. Royal Society of London (A)* **434**, 9-13.)

Lo, A.K. and McBean, G.A.: 1978, 'On the Relative Errors in Methods of Flux Calculations', *J. Appl. Meteorol.* **17**, 1704-1711.

Mahrt, L., Sun, J., Blumen, W., Delany, T. and Oncley, S.: 1998, 'Nocturnal Boundary-Layer Regimes', *Boundary-Layer Meteorol.* **88**, 255-278.

Monin, A.S. and Obukhov, A.M.: 1954 'Basic Laws of Turbulent Mixing in the Atmosphere Near the Ground', *Trudy Akad. Nauk S.S.S.R. Geofiz. Inst.* No. 24 **151**, 163-187.

Obukhov, A.M.: 1946, ‘Turbulence in an Atmosphere with Inhomogeneous Temperature’, *Trudy Inst. Teor. Geofiz. Akad. Nauk SSSR*. **1**, 95-115. (English transl. In: 1971, *Boundary-Layer Meteorol.* **3**, 7-29.)

Panofsky, H.A. and Dutton, J.A.: 1984, *Atmospheric Turbulence*, Wiley and Sons, New York, 397 pp.

Piccirillo, P. and Van Atta, C.W.: 1997, ‘The Evolution of a Uniformly Sheared Thermally Stratified Turbulent Flow’, *J. Fluid Mech.* **334**, 61-86.

Sreenivasan, K.R.: 1991,'On Local Isotropy of Passive Scalars in Turbulent Shear Flows', *Proc. Royal Society of London (A)* **434**, 165-182.

Stull, R.B.: 1988, *An Introduction to Boundary Layer Meteorology*, Kluwer, Dordrecht, NL, 666 pp.

Tennekes, H.: 1982, 'Similarity Relations, Scaling Laws and Spectral Dynamics', in F.T.M. Niewstadt and H. van Dop., (ed), *Atmospheric Turbulence and Air Pollution Modelling*, D. Reidel, Dordrecht, pp. 37-64.

Van Atta, C.: 1991, 'Local Isotropy of the Smallest Scales of Turbulent Scalar and Velocity Fields', *Proc. Royal Society of London (A)* **434**, 139-147.

World Meteorological Organization: 1998, ‘Commission for Instruments and Methods of Observation, Twelfth Session, Abridged Final Report with Resolutions and Recommendations’, *WMO Report No. 881*, Secretariat of the World Meteorological Organization, Geneva, Switzerland.

Wyngaard, J.C. and Cote', O.R.: 1972, 'Cospectral Similarity in the Atmospheric Surface Layer', *Quart. J. Roy. Meteorol. Soc.* **98**, 590-603.

Yee, E., Chan, R., Kosteniuk, P.R., Chandler, G.M., Biltoft, C.A. and Bowers, J.F.: 1995, ‘The Vertical Structure of Concentration fluctuation Statistics in Plumes Dispersing in the Atmospheric Surface Layer’, *Boundary-Layer Meteorol.* **76**, 41-67.